RDNAS: ROBUST DUAL-BRANCH NEURAL ARCHITECTURE SEARCH

Anonymous authors
Paper under double-blind review

ABSTRACT

Deep neural networks achieve impressive accuracy yet remain highly susceptible to adversarial perturbations, limiting their deployment in safety-critical domains. We propose **RDNAS**, a robust dual-branch neural architecture search framework that jointly optimizes standard (clean) accuracy and adversarial robustness. RDNAS introduces a dual-branch cell with separate "normal" and "robust" pathways, fused via a lightweight attention module to capture complementary representations without significantly enlarging the search space. To reliably score candidate operations under adversarial training, we develop **ROSE** (Robust Outlier-Aware Shapley Estimator), which stabilizes Shapley-based evaluation via median-of-means smoothing and interquartile-range filtering, reducing bias from noisy gradients. RDNAS consistently discovers architectures that outperform both hand-crafted networks and state-of-the-art robust NAS baselines across CIFAR-10, CIFAR-100, SVHN, and Tiny-ImageNet. Notably, it achieves 52.6% PGD^{20} robustness on CIFAR-10 while maintaining strong clean accuracy. Extensive ablations validate the effectiveness of the dual-branch design, attention-based fusion, and robustness-aware search. Overall, RDNAS provides a scalable and effective framework for discovering architectures resilient to adversarial attacks.

1 INTRODUCTION

Deep neural networks (DNNs) have achieved strong performance across vision tasks such as classification, segmentation, and detection (Krizhevsky et al., 2012; He et al., 2015). Yet their deployment in safety-critical domains—autonomous driving (Chen & Huang, 2017), medical imaging (Taigman et al., 2014), or biometric authentication—remains limited by their vulnerability to adversarial perturbations: small, imperceptible input changes that can drastically alter predictions. This fragility motivates research into adversarial robustness, where adversarial training (Madry et al., 2019; Zhang et al., 2019) is the prevailing defense. While effective, adversarial training alone cannot fully exploit robustness potential if the network architecture itself is not designed with robustness in mind.

Neural architecture search (NAS) offers a way to automatically discover architectures with strong performance. However, most NAS approaches—including differentiable (Heuillet et al., 2024; Yang et al., 2020; Chen et al., 2019b), zero-shot (Mellor et al., 2021; Peng et al., 2024), reinforcement learning (Zoph & Le, 2017; Baker et al., 2017), or evolutionary methods (Zhou et al., 2023; 2024)—optimize almost exclusively for clean accuracy, while treating robustness as secondary. Recent robust NAS studies (Simon et al., 2022; Feng et al., 2025a) incorporate adversarial training into the search loop, but typically score candidate operations via noisy adversarial gradients, leading to unstable updates and inconsistent robustness (Dong et al., 2025b; Cheng et al., 2023). For example, Shapley-based methods (Xiao et al., 2022) can be skewed by outliers, yielding unreliable attribution.

We propose **RDNAS** (Robust Dual-Branch NAS), a robustness-aware framework that jointly optimizes clean (standard) accuracy and adversarial robustness. RDNAS builds on three ideas: **(i)** A dual-branch cell that disentangles feature representation learning into a *normal* and a *robust* pathway, fused through a lightweight attention mechanism. Unlike ensembles or mixture-of-experts, this design does not duplicate operators or widen the search combinatorics; instead, it introduces a single extra dimension (one additional cell type) while keeping the operator set unchanged, thereby maintaining search efficiency. **(ii)** Adversarial training directly embedded in the inner loop of NAS, steering the search toward architectures that are in-

herently robust to perturbations. **(iii) ROSE** (Robust Outlier-Aware Shapley Estimator), a stabilized Shapley-based scoring mechanism that combines median-of-means smoothing with interquartile-range filtering to dampen gradient noise and reward rare but decisive operation effects. To keep the search tractable, we couple ROSE with a few-sample evaluation strategy that reduces both the supernet training and scoring costs, achieving stability without significant computational overhead. Moreover, inspired by robustness studies on wide architectures (Wu et al., 2025), RDNAS prioritizes width over depth, achieving resilience with fewer layers and similar parameter budgets to conventional NAS cells.

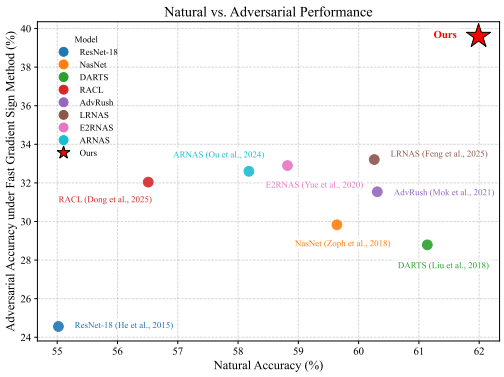

Figure 1: Clean vs. adversarial (FGSM) accuracy of various architectures on CIFAR-100. **Ours** achieves a favorable trade-off between robustness and clean performance, outperforming NAS-based and hand-crafted models.

We validate RDNAS on CIFAR-10 (Krizhevsky, 2009), CIFAR-100 (Krizhevsky, 2009), SVHN, and Tiny-ImageNet (Deng et al., 2009) against diverse adversarial attacks (including FGSM (Goodfellow et al., 2015), PGD (Madry et al., 2019), and transfer-based attacks (Papernot et al., 2017)). As shown in Figure 1, RDNAS consistently surpasses both hand-crafted and NAS baselines in clean and robust accuracy. Our contributions are threefold: **(i)** A dual-branch cell design that explicitly separates and fuses clean and robust pathways, providing complementary representations without inflating the search space. **(ii)** A robustness-aware scoring mechanism (ROSE) that stabilizes Shapley attribution under adversarial training through principled statistical techniques. **(iii)** Empirical evidence that RDNAS discovers architectures with superior robustness and accuracy across datasets and attacks, while maintaining computational efficiency.

To ensure both rigor and reproducibility, we complement our empirical study with **theoretical analysis** of the proposed estimator and **release full source code** and search logs in the appendix and supplementary material.

2 Related Work

2.1 Adversarial Robustness (Attacks vs. Defenses)

Deep neural networks (DNNs) have achieved remarkable performance across many tasks yet remain vulnerable to adversarial examples, i.e., small (often human-imperceptible) perturbations that can significantly alter model predictions. Adversarial attacks are commonly categorized into *white-box* and *black-box* settings. In the white-box case, the attacker assumes full access to model parameters and gradients: FGSM (Goodfellow et al., 2015) performs a fast single-step perturbation aligned with the loss gradient, whereas PGD (Madry et al., 2019) performs multi-step projected gradient ascent within an ℓ_∞ ball of radius ϵ and serves as a strong baseline for white-box evaluation. In the black-box case, attacks operate under limited information, relying either on transferability (adversarial examples crafted on a surrogate model) or on query-based methods that estimate gradients from model outputs. AutoAttack (Croce & Hein, 2020) provides a parameter-free evaluation suite that combines strong white-box attacks (APGD-CE/APGD-DLR, FAB) with a black-box component (Square), and is widely used as a reliable robustness benchmark.

To counter adversarial threats, a variety of defenses have been proposed. Among existing strategies, adversarial training has proven to be one of the most effective—in particular, PGD-based adversarial training, which is formulated as a min–max optimization between the model and the adversary. Notable extensions include TRADES (Zhang et al., 2019), which balances standard accuracy and robustness through a regularized loss. Despite these advances, the robustness of a model remains closely tied to its underlying architecture. Architectures not explicitly designed for robustness often exhibit an inherent trade-off between clean accuracy and adversarial performance. This observation underscores the need for robustness-aware NAS, where adversarial objectives are integrated directly into the search process.

2.2 Robustness-Aware Neural Architecture Search

Neural architecture search (NAS) automates the design of DNNs, optimizing trade-offs among accuracy, efficiency, and model complexity. Early efforts considered *macro-level* search over entire networks (Zoph & Le, 2017), followed by *micro-level* approaches that learn reusable cells and stack them to build full models (Pham et al., 2018). To improve scalability, DARTS (Liu et al., 2019) introduced a continuous relaxation that forms a Supernet with differentiable operation selection; subsequent variants such as GDAS (Dong & Yang, 2019b) and PC-DARTS (Xu et al., 2019) further improved the efficiency of gradient-based search.

While NAS has achieved strong results in clean settings, adversarial robustness has only recently become a central focus. Early work incorporated robustness into DARTS-style frameworks via adversarial training or robustness-aware objectives—e.g., smoothness priors, certified bounds, or Jacobian regularization—to guide the search (Guo et al., 2020a; Zela et al., 2020; Mok et al., 2021; Hosseini et al., 2021). Others explored broader search spaces, hybrid designs, and topological changes to improve robustness, revealing that simple strategies such as ensembling or width expansion can enhance adversarial accuracy (Vargas et al., 2019; Yang et al., 2024b; Devaguptapu et al., 2021; Liu et al., 2023). More recent methods adopt multi-objective formulations (Geraeinejad et al., 2021) to jointly consider accuracy, robustness, and efficiency, while designing specialized search spaces (Sun et al., 2025) and robustness-aware proxies (Jung et al., 2023). Additional strategies—including knowledge distillation (Nath et al., 2024), architectural disentanglement (Yang et al., 2024a), and adaptive channel allocation (Li et al., 2024)—further refine the search process (Chen et al., 2020). Meanwhile, techniques like Fair-DARTS (Chu et al., 2020) and BatchQuant (Bai et al., 2021) study robustness under constraints such as discretization and quantization.

Collectively, these developments reflect growing momentum toward NAS (especially DARTS-based) frameworks that explicitly optimize adversarial robustness across architectures and domains. Nevertheless, many approaches still depend on predefined templates and heuristic evaluations (e.g., PGD accuracy), which can introduce statistical noise and obscure robustness-critical factors. This motivates the need for principled, robustness-aware NAS frameworks that dynamically identify sensitivity in operations and architectural choices, enabling the discovery of inherently robust models.

2.3 Shapley Values in Architecture Search

The Shapley value, rooted in cooperative game theory (Nowak & Radzik, 1994), provides a principled way to assess the contribution of individual components to a collective reward. Let $N = \{1, \ldots, n\}$ index the components and let $v : 2^N \to \mathbb{R}$ assign a value to each subset $S \subseteq N$. The Shapley value of component $i \in N$ is

$$\phi_i(v) \;=\; \frac{1}{n!} \sum_{\pi \in \mathcal{P}(N)} \big[\, v(\mathrm{pre}_i(\pi) \cup \{i\}) - v(\mathrm{pre}_i(\pi)) \,\big], \tag{1}$$

where $\mathcal{P}(N)$ is the set of all permutations of N and $\mathrm{pre}_i(\pi)$ denotes the set of components preceding i in permutation π. Shapley-based approaches have been widely used for feature attribution and, more recently, for NAS (Xiao et al., 2022) to identify influential operations. AutoShape (Fang et al., 2023) and GraphNAP++ (Oloulade et al., 2025) apply Shapley-guided pruning or architecture selection. KernelSHAP-NAS (Tran et al., 2025) adapts KernelSHAP to approximate operation influence in a supernet more robustly than earlier sampling-based methods. D-DARTS (Heuillet et al., 2023) introduces a Shapley-based loss to guide distributed differentiable NAS, promoting diversity and cell-specific optimization. Beyond architecture search, SDL (Djenouri et al., 2023) leverages Shapley values for model consensus in general-purpose vision systems, and various algorithms have been proposed to estimate Shapley values more accurately and efficiently (Chen et al., 2023).

Nevertheless, effectiveness under adversarial evaluation can be hindered by high variance in marginal contributions due to input perturbations and limited sample sizes. To address this, we develop **ROSE** with two robust statistical techniques: the interquartile range (IQR) (Rousseeuw & Hubert, 2017), which flags outlier contributions using quartiles Q_1 and Q_3 (with IQR $= Q_3 - Q_1$), and the median-of-means (MoM) estimator (Lecué & Lerasle, 2017). These tools yield a more stable and robust estimation pipeline for operation importance under adversarial noise. This design grounds ROSE in established statistical principles while extending Shapley-based NAS to adversarial settings for the first time; we further provide detailed theoretical analysis in the appendix.

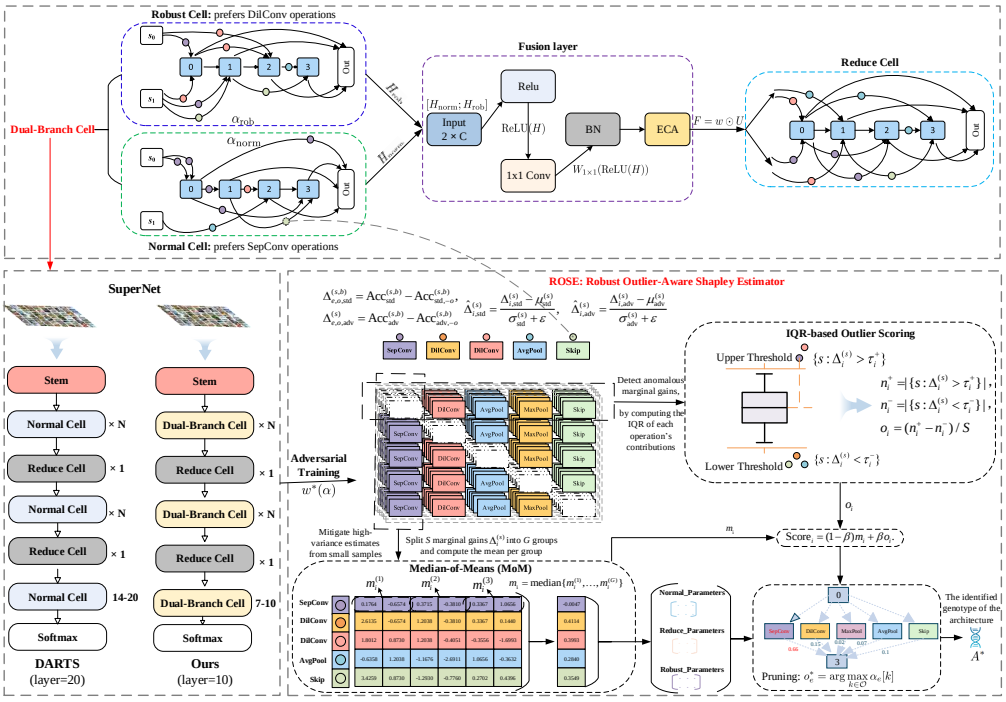

Figure 2: Overview of the RDNAS framework: (left) the dual-branch cell design; (middle) a comparison between standard DARTS (20 layers) and our dual-branch network (10 layers); (right) the ROSE estimator.

3 Methodology

3.1 Overview of RDNAS

RDNAS follows the DARTS paradigm in which an architecture is built by stacking cells—directed acyclic graphs (DAGs) with N intermediate nodes and a predefined operation set $\mathcal{O}$ (e.g., depthwise convolutions, pooling, identity). For each edge (i, j), we maintain logits $\boldsymbol{\alpha}^{(i,j)} = \{\alpha_o^{(i,j)}\}_{o\in\mathcal{O}}$ that parameterize a softmax mixture of operations:

$$\tilde{o}^{(i,j)}\big(x^{(i)}\big) = \sum_{o\in\mathcal{O}} \frac{\exp(\alpha_o^{(i,j)})}{\sum_{o'\in\mathcal{O}} \exp(\alpha_{o'}^{(i,j)})}\, o\Big(x^{(i)}\Big). \tag{2}$$

As illustrated in Figure 2, we enhance the standard DARTS backbone—typically 20 normal cells and 2 reduction cells—by replacing each normal cell with a *dual-branch* cell while halving the depth (10 dual-branch cells plus 2 reduction cells). The two branches process features in parallel to emphasize clean and robust pathways, respectively; at each fusion point an *Efficient Channel Attention* (ECA) module adaptively reweights and aggregates channel-wise responses, enabling selective retention of informative representations (see Appendix A.2 for Grad-CAM visualizations). The final representation is fed to a softmax classifier.

To support efficient search, we relax discrete operation choices into continuous architecture parameters α and jointly optimize network weights ω and α via bilevel optimization:

$$\min_{\alpha}\ \mathcal{L}_{\text{val}}\big(\omega^*(\alpha), \alpha\big), \tag{3}$$

$$\text{s.t. } \omega^*(\alpha) = \arg\min_{\omega}\ \mathcal{L}_{\text{train}}(\omega, \alpha), \tag{4}$$

where the inner objective adopts a composite loss on clean and adversarial examples,

$$\mathcal{L}_{\text{train}} = \lambda \cdot \mathcal{L}_{\text{clean}} + (1-\lambda)\cdot \mathcal{L}_{\text{adv}}. \tag{5}$$

(details in Sec. 4.2), and the outer objective is evaluated under the same robustness settings. RDNAS employs robustness-aware bilevel optimization to balance accuracy and adversarial resilience.

To improve stability under noisy gradients, we introduce **ROSE**, which scores operations on each edge (i, j) and guides lightweight pruning. By combining MoM smoothing with IQR filtering, ROSE yields robust importance estimates. After convergence, we discretize by retaining the top operation(s) per edge based on ROSE scores, producing a compact model that balances clean accuracy and adversarial robustness.

3.2 Dual-Branch Cell Design

Conventional gradient-based NAS methods (e.g., DARTS) rely on a *single* shared cell to process both clean and adversarial data. Under adversarial training, this shared cell must simultaneously serve two competing objectives, and we empirically observe that the resulting architectures tend to favor either clean accuracy or robustness, but rarely both. Although one could attempt a single cell with a composite loss (e.g., TRADES (Zhang et al., 2019)), we find that explicitly separating the optimization paths allows each branch to specialize, leading to superior overall performance. This design reduces interference between objectives and provides more stable architecture search under adversarial training.

To this end, we introduce the *Dual-Branch Cell*, which decouples learning into two parallel subnetworks: a normal branch for clean accuracy and a robust branch for adversarial resilience. Both branches process the same inputs (s_0, s_1) using a shared operator class $\mathcal{C}$ but independent architecture parameters α_{norm} and α_{rob}:

$$H_{\text{norm}} = \mathcal{C}(s_0, s_1; \alpha_{\text{norm}}), \quad H_{\text{rob}} = \mathcal{C}(s_0, s_1; \alpha_{\text{rob}}), \tag{6}$$

where $H_{\text{norm}}, H_{\text{rob}} \in \mathbb{R}^{C\times H\times W}$. Their outputs are concatenated along the channel dimension to form a joint representation:

$$H = [H_{\text{norm}}; H_{\text{rob}}] \in \mathbb{R}^{2C\times H\times W}. \tag{7}$$

Naively fusing both branches without weighting treats clean and robust features as equally important at all times, which can limit expressiveness. To more effectively exploit the complementary representations, we adopt an attention-based fusion mechanism inspired by Efficient Channel Attention (ECA) (Wang et al., 2020). First, we reduce the channel dimension with a 1×1 convolution followed by ReLU activation:

$$U = W_{1\times 1}(\text{ReLU}(H)) \in \mathbb{R}^{C\times H\times W}. \tag{8}$$

Next, global average pooling extracts a compact channel descriptor:

$$z = \text{GAP}(U) \in \mathbb{R}^{C}, \tag{9}$$

which is passed through a 1D convolution (with an adaptively determined kernel size as in ECA) and a sigmoid activation to generate channel-wise attention weights:

$$w = \sigma(\text{Conv1D}(z)) \in (0, 1)^{C}. \tag{10}$$

These weights modulate the feature map via element-wise multiplication:

$$F = w \odot U \in \mathbb{R}^{C\times H\times W}. \tag{11}$$

The fused output F is forwarded to the next layer. By explicitly separating optimization paths and adaptively fusing them, the Dual-Branch Cell encourages each branch to specialize: the normal branch can focus on fine-grained discriminative patterns, while the robust branch learns smoother, perturbation-insensitive structures. This reduces conflict between clean and robust objectives and stabilizes architecture search. Our ablation in Table 4 shows that introducing ECA-based fusion consistently improves both clean and PGD^{20} accuracy over a dual-branch design without attention. Moreover, Grad-CAM visualizations in Appendix A.2 qualitatively confirm that the two branches attend to different yet complementary regions under clean and adversarial inputs, providing empirical evidence that the dual-branch design effectively captures diverse features.

3.3 Adversarially Robust Search

Following recent advances in robust NAS, we integrate adversarial training directly into the inner optimization loop to promote robustness-aware search. While conventional DARTS assumes subnet

Algorithm 1 Adversarially Robust Architecture Search

Input: Search space $\mathcal{S} = \{o_{ij}\}$, warm-up epochs N_w, search epochs N_s, #Shapley samples S, #MoM groups G, IQR sensitivity γ, training data D_{train}, validation data D_{val}
Output: Adversarially robust architecture A^*
Initialize architecture logits $\alpha_n \in \mathbb{R}^{E\times O}$ for each branch $b \in \{\text{normal}, \text{reduce}, \text{robust}\}$ and weights ω;
for epoch = 1 **to** $N_w + N_s$ **do**
  Train ω on D_{train} by minimize the composite training loss in (5);
  if epoch $> N_w$ **then**
    Compute the clean and adversarial accuracy deltas $\Delta^{(s,b)}_{e,o,\text{std}}$ and $\Delta^{(s,b)}_{e,o,\text{adv}}$ by (15);
    Compute the final $\text{Score}^{(b)}_{e,o}$ by ROSE in (19) based on (15) to (18);
    Update logits: $\alpha \leftarrow \alpha + \eta \cdot \text{Score}$;
    Row-normalize each edge of α so its logits sum to 1;
  end if
end for
Pick the operation for each edge with highest logit to form A^*;
Return: A^*

ranking is consistent between small-search and large-inference networks, this assumption often fails under adversarial training due to high-variance gradients. To address this, we leverage ROSE as a statistically stable operation scorer, which mitigates the effect of noisy gradients and provides reliable guidance for architecture updates.

Specifically, during each epoch, clean inputs x are transformed into adversarial examples x^{adv} using a fast PGD-k method (e.g., $k = 7$ steps):

$$x^{\text{adv}} = \arg\max_{\|\delta\|_\infty \le \epsilon} \mathcal{L}_{\text{train}}(f(x+\delta), y), \tag{12}$$

where ϵ constrains the perturbation magnitude and $\mathcal{L}_{\text{train}}$ is the composite training loss that mitigates overfitting to clean samples and steers weight learning toward robust representations.

After obtaining the optimal network weights $w^*(\alpha)$, the outer optimization fixes $w^*(\alpha)$ and updates architecture parameters α by minimizing the ROSE-weighted validation loss:

$$\mathcal{L}_{\text{val}}\big(w^*(\alpha), \alpha\big) \;=\; -\sum_{b=1}^{3}\sum_{e=1}^{E}\sum_{o=1}^{O} p^{(b)}_{e,o}(\alpha)\,\text{Score}^{(b)}_{e,o} \tag{13}$$

where b indexes normal, reduce, and robust branches, and $p^{(b)}_{e,o}(\alpha) = \text{softmax}\big(\alpha^{(b)}_{e,\cdot}\big)_o$ is the probability of selecting operation o on edge e of branch b. The ROSE score $\text{Score}^{(b)}_{e,o}$ stabilizes operation evaluation under noisy adversarial gradients, ensuring that the outer-loop update favors consistently robust operations.

Upon convergence, architecture discretization selects the most probable operation per edge:

$$o^*_e = \arg\max_{k\in\mathcal{O}} \alpha_e[k] \tag{14}$$

The resulting normal and robust cells are paired into Dual-Branch Cells, interleaved with Reduce Cells, and stacked to form a compact backbone that balances clean accuracy and adversarial robustness. To reduce search cost and maintain practical efficiency, we adopt a small-sample search strategy: only a fraction of the training data is used per search epoch, which, combined with lightweight 10-cell networks, drastically reduces computation while preserving ranking stability under ROSE guidance. The overall search procedure is summarized in Algorithm 1. This setup ensures that RDNAS discovers robust architectures efficiently, mitigating both the DARTS-related ranking inconsistencies and the high computational overhead of adversarial training.

3.4 ROSE: Robust Outlier-Aware Shapley Estimator

After revisiting the Shapley foundations, we find that certain operations disproportionately influence adversarial robustness. However, under adversarial training, architecture evaluation is inherently noisy: gradient estimates fluctuate due to stochastic perturbations, and individual operations may

appear important or unimportant depending on the sampled adversarial examples. This motivates ROSE, which refines Shapley-based scoring to capture both stable contributions and rare but critical effects. Unlike conventional approaches that score all operations jointly, ROSE applies separate evaluations to the normal, reduction, and robust cells, yielding three branch-specific score matrices. By decoupling branches, ROSE also preserves branch-specific sensitivity, aligning with our dual-branch cell design.

ROSE enhances the standard Monte Carlo Shapley sampler using two complementary techniques: 1) *IQR-based outlier detection*, operations whose standardized marginal gains fall outside the interquartile range are highlighted, allowing rare yet decisive contributions to be recognized rather than averaged away. This helps capture edges that are critical under adversarial conditions. 2) *MoM smoothing*, by partitioning permutations into groups and aggregating their means, MoM reduces the variance introduced by stochastic gradients, producing a stable Shapley estimate that reliably ranks operations across noisy adversarial evaluations.

Let $b \in \{\text{normal}, \text{reduce}, \text{robust}\}$ index each cell branch, and $\mathcal{O}^{(b)}$ denote its candidate operations, with the rest of the supernet fixed. Over S random permutations, we compute clean and adversarial accuracy deltas for each operation o on edge e in branch b:

$$\Delta^{(s,b)}_{e,o,\text{std}} = \text{Acc}^{(s,b)}_{\text{std}} - \text{Acc}^{(s,b)}_{\text{std},-o}, \quad \Delta^{(s,b)}_{e,o,\text{adv}} = \text{Acc}^{(s,b)}_{\text{adv}} - \text{Acc}^{(s,b)}_{\text{adv},-o} \tag{15}$$

where $\text{Acc}^{(s,b)}_{\text{std}}$ (or $\text{Acc}^{(s,b)}_{\text{adv}}$) denotes validation accuracy with operation o, and $\text{Acc}^{(s,b)}_{\text{std},-o}$ (or $\text{Acc}^{(s,b)}_{\text{adv},-o}$) denotes the accuracy after removing o. These deltas are standardized per permutation to reduce variance:

$$\hat{\Delta}^{(s)}_{i,\text{std}} = \frac{\Delta^{(s)}_{i,\text{std}} - \mu^{(s)}_{\text{std}}}{\sigma^{(s)}_{\text{std}} + \epsilon}, \quad \hat{\Delta}^{(s)}_{i,\text{adv}} = \frac{\Delta^{(s)}_{i,\text{adv}} - \mu^{(s)}_{\text{adv}}}{\sigma^{(s)}_{\text{adv}} + \epsilon} \tag{16}$$

where $\mu^{(s)}$ and $\sigma^{(s)}$ are empirical statistics across operations, and ϵ ensures numerical stability.

To capture anomalies, we compute the IQR for each $\{\hat{\Delta}^{(s,b)}_{e,o}\}_{s=1}^{S}$, set upper and lower thresholds $\tau^{(b)+}_{e,o}$ and $\tau^{(b)-}_{e,o}$, and derive an outlier score:

$$v^{(b)}_{e,o} = \frac{\left|\{s : \hat{\Delta}^{(s,b)}_{e,o} > \tau^{(b)+}_{e,o}\}\right| - \left|\{s : \hat{\Delta}^{(s,b)}_{e,o} < \tau^{(b)-}_{e,o}\}\right|}{S} \tag{17}$$

Here, $v^{(b)}_{e,o} > 0$ suggests frequent robustness gains when o is dropped, while $v^{(b)}_{e,o} < 0$ indicates critical importance.

For stability, the MoM estimate is computed by partitioning samples into G folds, averaging within each fold, and taking the median:

$$m^{(b)}_{e,o} = \text{median}\Big\{\frac{1}{|\mathcal{G}_k|}\sum_{s\in\mathcal{G}_k}\hat{\Delta}^{(s,b)}_{e,o}\Big\}_{k=1}^{G} \tag{18}$$

Intuitively, MoM ensures that the ranking of operations is not dominated by extreme but noisy gradients, while IQR ensures that rare but impactful operations are not ignored. This combination provides a principled, statistically robust evaluation of each candidate.

The final ROSE score combines both components:

$$\text{Score}^{(b)}_{e,o} = (1-\beta)\, m^{(b)}_{e,o} + \beta\, v^{(b)}_{e,o} \tag{19}$$

where $\beta \in [0,1]$ balances *steady reward* and *occasional indispensability*. Empirically, $\beta \in [0.3, 0.5]$ yields architectures that are both reliably accurate and resilient under adversarial conditions, demonstrating that ROSE effectively guides the search toward robust-optimal configurations.

We use the ROSE score to rank (and, if enabled, lightly prune) candidate operations in each cell. This selective mechanism stabilizes operation evaluation under noisy adversarial training and highlights components that are consistently valuable or occasionally critical, providing a clear justification for ROSE's necessity. Sensitivity experiments on β are presented in Sec. A.3, with additional hyperparameter studies for the entire framework provided in Appendix A.3.

4 EXPERIMENTAL STUDIES

4.1 BENCHMARK DATASETS AND BASELINES

Following established practices in robust NAS research (Guo et al., 2019; Mok et al., 2021), we evaluate our proposed method, RDNAS, on four benchmark datasets: CIFAR-10, CIFAR-100 (Krizhevsky, 2009), SVHN, and Tiny-ImageNet-200 (Le & Yang, 2015).

We compare RDNAS against a comprehensive set of peer methods, including manually designed architectures such as ResNet-18 (He et al., 2015) and DenseNet-121 (Huang et al., 2017), standard NAS frameworks like DARTS (Liu et al., 2019), NASNet (Zoph et al., 2018), and PDARTS (Chen et al., 2019a), GDAS (Dong & Yang, 2019b), SETN (Dong & Yang, 2019a), and ENAS (Pham et al., 2018); training-free NAS baselines including TTNAS (Lin et al., 2024) and MOTE-NAS (Zhang et al., 2024); as well as robust NAS approaches such as RobNet (Guo et al., 2020b), AdvRush (Mok et al., 2021), RACL (Dong et al., 2025a), E2RNAS (Yue et al., 2020), ARNAS (Ou et al., 2024), and LRNAS (Feng et al., 2025a). We ensure fair comparisons by reporting FLOPs and parameter counts for all baselines, highlighting that improvements of RDNAS are achieved under comparable or lower computational budgets.

4.2 SEARCH CONFIGURATION AND EVALUATION PROTOCOL

Given that RDNAS adopts a shallower architecture, we conduct the search on a 10-cell network (instead of 8) and *adjust* the initial channel count to 32 (the common setting is 36) to maintain training–search consistency. The search runs for 50 epochs using adversarial training based on 7-step PGD with a step size of $2/255$ and perturbation bound of $8/255$. The adversarial loss regularization coefficient is set to 0.5. Other settings follow DARTS. Network weights (ω) are optimized using SGD with momentum 0.9, learning rate $\eta_w = 0.025$ (cosine decay), and weight decay 3×10^{-4}. Architecture parameters (α) use Adam with $\eta_\alpha = 3 \times 10^{-4}$, $\beta = (0.5, 0.999)$, and weight decay 10^{-3}. To substantially reduce search cost and accelerate convergence under adversarial training, we adopt a small-sample search: on CIFAR-10, only 1,000 training samples and 500 validation samples are used. **ROSE is critical here**, as it stabilizes architecture ranking under small-sample noisy gradients, enabling reliable discovery of robust architectures in a fraction of typical search time. To the best of our knowledge, this is the first attempt to combine small-sample one-shot NAS with adversarial training.

For final evaluation, we stack 10 cells with an initial channel count of 32. Stem / Reduction-1 / Reduction-2 channels are set to 32 / 128 / 128. Following AdvRush (Mok et al., 2021), we adversarially train each model for 120 epochs using 7-step PGD (step size 0.01, $\epsilon = 8/255$). Optimization uses SGD with momentum 0.9 and weight decay 1×10^{-4}. Learning rates are 0.1 (CIFAR-10/100) and 0.01 (SVHN), decayed at epochs 90 and 104. Batch size is 32. All experiments are performed on an NVIDIA GeForce RTX 4080 Super GPU.

Table 1: Robust accuracy on CIFAR-10. All attacks use ℓ_∞ budget $\epsilon = 8/255$. Columns report clean (Nat.) and white-box attacks; the last two columns show AutoAttack (AA) and GPU-days. Best in each column is **bold**.

Model	Params	FLOPs	Evaluation (ℓ_∞)					AA	GPUday
			Nat.	FGSM	PGD^{20}	PGD^{100}	APGD-CE		
ResNet-18	11.2M	37.67M	84.09%	54.64%	45.86%	45.53%	44.54%	43.22%	–
DenseNet-121	7.0M	59.83M	85.95%	58.46%	50.49%	49.92%	49.11%	47.46%	–
DARTS	3.3M	547.44M	85.92%	58.96%	51.45%	49.32%	48.32%	47.73%	1.0
PDARTS	3.4M	550.75M	85.38%	59.12%	51.32%	50.91%	49.96%	48.52%	0.3
RobNet	5.6M	800.40M	85.00%	59.22%	52.09%	51.14%	50.41%	48.56%	3.3
DSRNA	2.0M	336.23M	80.93%	54.49%	49.11%	48.89%	48.67%	44.87%	0.4
LRNAS	2.2M	346.10M	84.26%	59.89%	50.20%	49.90%	49.83%	49.07%	0.4
RACL	3.6M	568.86M	85.13%	59.45%	51.89%	51.63%	51.09%	**50.23%**	0.5
AdvRush	4.2M	668.53M	86.38%	60.32%	52.29%	51.80%	51.42%	50.05%	0.7
RDNAS (Ours)	4.4M	1.30G	**86.56%**	**60.44%**	**52.62%**	**52.24%**	**52.05%**	49.98%	0.2

Table 2: Transfer-based black-box accuracy on CIFAR-10/100 (%).

Dataset	Params (M)	Source	Target					
			DARTS	AdvRush	LRNAS	RACL	PDARTS	Ours
CIFAR-10	3.3	DARTS	–	65.22	63.01	65.22	66.21	**67.54**
	4.2	AdvRush	65.40	–	63.52	65.45	66.29	**67.60**
	2.3	LRNAS	67.96	68.67	–	67.83	68.92	**69.46**
	3.6	RACL	65.44	65.46	62.54	–	64.97	**65.80**
	3.4	PDARTS	65.25	65.24	62.61	63.81	–	**65.52**
	4.4	Ours	**67.16**	66.80	63.85	65.79	66.32	–
CIFAR-100	3.3	DARTS	–	43.63	42.78	43.29	40.17	**46.37**
	4.2	AdvRush	42.46	–	41.91	42.83	40.01	**46.54**
	2.8	LRNAS	43.35	44.27	–	44.73	41.87	**47.06**
	3.6	RACL	42.68	41.83	42.25	–	40.39	**46.72**
	3.4	PDARTS	40.06	41.39	38.38	40.71	–	**45.94**
	4.4	Ours	47.04	**47.83**	44.61	47.65	47.18	–

Table 3: Cross-dataset transfer results (%, ϵ=$8/255$, PGD^{20} step size $2/255$). Best result in each sub-table is **bold**.

CIFAR-100

Model	Clean	FGSM	PGD^{20}
ResNet-18	55.57	26.03	21.44
AdvRush	60.31	31.54	27.38
RACL	59.18	34.40	**30.41**
ARNAS	58.18	32.60	29.54
RDNAS	**61.99**	**39.60**	29.42

SVHN

Model	Clean	FGSM	PGD^{20}
ResNet-18	92.06	88.73	69.51
DenseNet-121	95.10	93.01	89.58
ARNAS	95.84	94.43	92.02
AdvRush	96.53	94.95	91.14
RDNAS	**97.88**	**96.37**	**95.80**

Tiny-ImageNet-200

Model	Clean	FGSM	PGD^{20}
ResNet-18	36.26	16.08	13.94
DenseNet-121	47.56	22.98	18.06
PDARTS	45.94	24.36	22.74
AdvRush	46.42	24.20	**22.89**
RDNAS	**56.84**	**24.49**	19.40

4.3 Results on White-box Attacks

Table 1 shows that **RDNAS** attains the strongest overall white-box results: it is best on Clean, FGSM, PGD^{20}, PGD^{100}, and APGD-CE, and only 0.25 pp behind the best prior AutoAttack score (49.98% vs. 50.23% for RACL), with a moderate 4.4M parameters. Our FLOPs (1.30G) are higher than some DARTS-style baselines due to the dual-branch design with ECA fusion, but this extra compute yields consistent gains across all white-box attacks. The cost is practical: the search budget is small (0.2 GPU-days), and the halved depth (10 cells) helps latency despite per-cell compute. Moreover, the robustness *transfers*: Table 2 shows best or tied-best transfer-based black-box performance in most source→target pairs, and Table 3 confirms strong cross-dataset results (CIFAR-100, SVHN, Tiny-ImageNet-200). Overall, the modest FLOPs increase buys attack- and dataset-general robustness, making the accuracy–compute trade-off favorable.

4.4 Results on Black-box Attacks

We evaluate transfer-based black-box robustness on CIFAR-10 and CIFAR-100 using adversarial examples generated by PGD (untargeted, $\epsilon = 8/255$, step size $2/255$, 20 steps, random starts) from five source models: DARTS, PDARTS, RACL, LRNAS, and AdvRush. Unless otherwise noted, attacks are single-source transfers (no ensemble). As summarized in Table 2, RDNAS outperforms peers in most transfer settings. Notably on CIFAR-100, it retains top robustness when attacked by adversarial inputs generated from the above sources. Despite its moderate size (4.4M parameters), RDNAS achieves 65.5%–69.5% robust accuracy on CIFAR-10 and 45.9%–47.8% on CIFAR-100, offering favorable robustness–parameter trade-offs relative to smaller models.

4.5 Cross-Dataset Transferability

To test generalization, we transfer the RDNAS architecture searched on CIFAR-10 to CIFAR-100, SVHN, and Tiny-ImageNet-200, and retrain from scratch on each target dataset (no re-search). As shown in Table 3, RDNAS attains strong clean and adversarial accuracies. On CIFAR-100, it surpasses ResNet-18 and NASNet in robustness; on SVHN, it achieves 97.88% clean accuracy and 96.37% FGSM robustness; on Tiny-ImageNet-200, it delivers 56.84% clean accuracy and remains competitive under PGD, trailing AdvRush slightly.

Table 4: Ablation of ECA, adversarial-training during search, and search space. Metrics are Top-1 (%) on clean and **PGD**^{20} ($\epsilon = 8/255$, step size $2/255$); Params in millions.

ID	ECA	Adv. search	Search space	Params (M)	Clean (%)	PGD^{20} (%)
A	×	×	Single Cell (20 cells)	4.20	84.8	50.3
B	×	✓	Single Cell (20 cells)	4.28	85.6	51.0
C	✓	✓	Single Cell (20 cells)	4.30	86.0	51.5
D	×	✓	Dual-Branch Cell (10 cells)	4.26	85.7	51.8
E	✓	✓	Dual-Branch Cell (10 cells)	4.32	**86.5**	**52.6**

4.6 Ablation Studies

Search-Space Ablation: As shown in Table 4, a reduced RDNAS search space (10 operations) outperforms the full DARTS space (20 operations) under FGSM and PGD, while maintaining similar clean accuracy. This demonstrates that our carefully designed operation set suffices for robust architecture discovery and reduces search complexity.

Adversarial Training Ablation: Clean-only search yields strong natural accuracy but poor PGD robustness. Integrating adversarial training during search significantly improves robustness, validating its importance.

Attention Module Ablation: Removing the Efficient Channel Attention (ECA) module slightly degrades clean accuracy and noticeably reduces adversarial robustness. Reintroducing ECA improves both, confirming its effectiveness. Grad-CAM visualizations (Appendix A.2) further show that the two branches focus on complementary regions, providing qualitative support for the attention module's role in robust feature integration.

ROSE Ablation: ROSE is enabled by default in our adversarial-search setting. To assess its contribution, we run an additional search variant without ROSE, using standard Shapley estimates. This variant shows higher run-to-run variability and slightly lower PGD robustness, indicating that ROSE stabilizes small-sample adversarial NAS and aids in discovering architectures with more consistent robust performance.

4.7 Results on NAS-Bench-201 (CIFAR-10)

Table 5 reports validation/test accuracy and search cost on NAS-Bench-201 (CIFAR-10). We list classic gradient-based baselines and recent training/evaluation-free methods (e.g., TTNAS (Lin et al., 2024), MOTE-NAS (Zhang et al., 2024)). Our method achieves the best trade-off between accuracy and search time. This experiment demonstrates that, even under a few-sample search regime, the ROSE estimator remains stable and reliably discovers robust architectures.

Method	Search (s)	val	test
DARTS-V2	35781.80	39.77±0.00	54.30±0.00
GDAS	31609.80	89.89±0.08	93.61±0.09
SETN	34139.53	84.04±0.28	87.64±0.00
ENAS	14058.80	37.51±3.19	53.89±0.58
TTNAS (training-free)	1146	91.02±0.11	93.94±0.38
MOTE-NAS (K=5)	2239	90.89±0.13	93.86±0.15
Ours	**731**	**91.13±0.36**	**93.97±0.35**
Ground Truth	—	**91.61**	**94.37**

Table 5: Validation and test accuracy with corresponding search cost on NAS-Bench-201 (CIFAR-10). RDNAS achieves the best trade-off between accuracy and efficiency, demonstrating stable performance even under limited search budgets.The results include the average and standard deviations for 3 runs.

5 Conclusion

This work presents RDNAS, a robust NAS framework that jointly optimizes for accuracy and adversarial robustness. We propose a dual-branch cell search space and enhance Shapley-value estimation using MoM and IQR to identify critical operations. Extensive experiments across multiple benchmarks and attack settings demonstrate the effectiveness and transferability of RDNAS, with results highlighting that heterogeneous cell placement across depths is crucial for balancing robustness and accuracy.

REFERENCES

Haoping Bai, Meng Cao, Ping Huang, and Jiulong Shan. Batchquant: Quantized-for-all architecture search with robust quantizer. *Advances in Neural Information Processing Systems*, 34:1074–1085, 2021.

Bowen Baker, Otkrist Gupta, Nikhil Naik, and Ramesh Raskar. Designing neural network architectures using reinforcement learning, 2017. URL https://arxiv.org/abs/1611.02167.

Hanlin Chen, Baochang Zhang, Song Xue, Xuan Gong, Hong Liu, Rongrong Ji, and David Doermann. Anti-bandit neural architecture search for model defense. In *European conference on computer vision*, pp. 70–85. Springer, 2020.

Hugh Chen, Ian C Covert, Scott M Lundberg, and Su-In Lee. Algorithms to estimate shapley value feature attributions. *Nature Machine Intelligence*, 5(6):590–601, 2023.

Xin Chen, Lingxi Xie, Jun Wu, and Qi Tian. Progressive differentiable architecture search: Bridging the depth gap between search and evaluation. In *2019 IEEE/CVF International Conference on Computer Vision (ICCV)*, pp. 1294–1303, 2019a. doi: 10.1109/ICCV.2019.00138.

Xin Chen, Lingxi Xie, Jun Wu, and Qi Tian. Progressive differentiable architecture search: Bridging the depth gap between search and evaluation, 2019b. URL https://arxiv.org/abs/1904.12760.

Zhilu Chen and Xinming Huang. End-to-end learning for lane keeping of self-driving cars. In *2017 IEEE Intelligent Vehicles Symposium (IV)*, pp. 1856–1860, 2017. doi: 10.1109/IVS.2017.7995975.

Zhi Cheng, Yanxi Li, Minjing Dong, Xiu Su, Shan You, and Chang Xu. Neural architecture search for wide spectrum adversarial robustness. In *Proceedings of the AAAI Conference on Artificial Intelligence*, volume 37, pp. 442–451, 2023.

Xiangxiang Chu, Tianbao Zhou, Bo Zhang, and Jixiang Li. Fair darts: Eliminating unfair advantages in differentiable architecture search. In *European conference on computer vision*, pp. 465–480. Springer, 2020.

Francesco Croce and Matthias Hein. Reliable evaluation of adversarial robustness with an ensemble of diverse parameter-free attacks, 2020. URL https://arxiv.org/abs/2003.01690.

Jia Deng, Wei Dong, Richard Socher, Li-Jia Li, Kai Li, and Li Fei-Fei. Imagenet: A large-scale hierarchical image database. In *2009 IEEE Conference on Computer Vision and Pattern Recognition*, pp. 248–255, 2009. doi: 10.1109/CVPR.2009.5206848.

Chaitanya Devaguptapu, Devansh Agarwal, Gaurav Mittal, Pulkit Gopalani, and Vineeth N Balasubramanian. On adversarial robustness: A neural architecture search perspective. In *Proceedings of the IEEE/CVF international conference on computer vision*, pp. 152–161, 2021.

Youcef Djenouri, Ahmed Nabil Belbachir, Tomasz Michalak, and Anis Yazidi. Shapley deep learning: A consensus for general-purpose vision systems. In *Proceedings of the IEEE/CVF International Conference on Computer Vision*, pp. 1224–1233, 2023.

Minjing Dong, Yanxi Li, Yunhe Wang, and Chang Xu. Adversarially robust neural architectures. *IEEE Transactions on Pattern Analysis and Machine Intelligence*, 47(5):4183–4197, 2025a. doi: 10.1109/TPAMI.2025.3542350.

Minjing Dong, Yanxi Li, Yunhe Wang, and Chang Xu. Adversarially robust neural architectures. *IEEE Transactions on Pattern Analysis and Machine Intelligence*, 2025b.

Xuanyi Dong and Yi Yang. One-shot neural architecture search via self-evaluated template network. In *2019 IEEE/CVF International Conference on Computer Vision (ICCV)*. IEEE, October 2019a. doi: 10.1109/iccv.2019.00378. URL http://dx.doi.org/10.1109/ICCV.2019.00378.

Xuanyi Dong and Yi Yang. Searching for a robust neural architecture in four gpu hours. In *Proceedings of the IEEE/CVF conference on computer vision and pattern recognition*, pp. 1761–1770, 2019b.

Yunfei Fang, Caihong Mu, and Yi Liu. Autoshape: Automatic design of click-through rate prediction models using shapley value. In *Pacific Rim International Conference on Artificial Intelligence*, pp. 29–40. Springer, 2023.

Yuqi Feng, Zeqiong Lv, Hongyang Chen, Shangce Gao, Fengping An, and Yanan Sun. Lrnas: Differentiable searching for adversarially robust lightweight neural architecture. *IEEE Transactions on Neural Networks and Learning Systems*, 36(3):5629–5643, 2025a. doi: 10.1109/TNNLS.2024.3382724.

Yuqi Feng, Yuwei Ou, Jiahao Fan, and Yanan Sun. Zero-cost proxy for adversarial robustness evaluation. In *The Thirteenth International Conference on Learning Representations*, 2025b. URL https://openreview.net/forum?id=zHf7hOfeer.

Vahid Geraeinejad, Sima Sinaei, Mehdi Modarressi, and Masoud Daneshtalab. Roco-nas: Robust and compact neural architecture search. In *2021 International Joint Conference on Neural Networks (IJCNN)*, pp. 1–8. IEEE, 2021.

Ian J. Goodfellow, Jonathon Shlens, and Christian Szegedy. Explaining and harnessing adversarial examples, 2015. URL https://arxiv.org/abs/1412.6572.

Minghao Guo, Yuzhe Yang, Rui Xu, Ziwei Liu, and Dahua Lin. When nas meets robustness: In search of robust architectures against adversarial attacks. *arXiv preprint arXiv:1911.10695*, 2019.

Minghao Guo, Yuzhe Yang, Rui Xu, Ziwei Liu, and Dahua Lin. When nas meets robustness: In search of robust architectures against adversarial attacks. In *Proceedings of the IEEE/CVF conference on computer vision and pattern recognition*, pp. 631–640, 2020a.

Minghao Guo, Yuzhe Yang, Rui Xu, Ziwei Liu, and Dahua Lin. When nas meets robustness: In search of robust architectures against adversarial attacks, 2020b. URL https://arxiv.org/abs/1911.10695.

Hyeonjeong Ha, Minseon Kim, and Sung Ju Hwang. Generalizable lightweight proxy for robust nas against diverse perturbations, 2023. URL https://arxiv.org/abs/2306.05031.

Kaiming He, Xiangyu Zhang, Shaoqing Ren, and Jian Sun. Deep residual learning for image recognition, 2015. URL https://arxiv.org/abs/1512.03385.

Alexandre Heuillet, Hedi Tabia, Hichem Arioui, and Kamal Youcef-Toumi. D-darts: Distributed differentiable architecture search. *Pattern Recognition Letters*, 176:42–48, 2023.

Alexandre Heuillet, Ahmad Nasser, Hichem Arioui, and Hedi Tabia. Efficient automation of neural network design: A survey on differentiable neural architecture search. *ACM Computing Surveys*, 56(11):1–36, 2024.

Ramtin Hosseini, Xingyi Yang, and Pengtao Xie. Dsrna: Differentiable search of robust neural architectures. In *Proceedings of the IEEE/CVF Conference on Computer Vision and Pattern Recognition*, pp. 6196–6205, 2021.

Gao Huang, Zhuang Liu, Laurens Van Der Maaten, and Kilian Q. Weinberger. Densely connected convolutional networks. In *2017 IEEE Conference on Computer Vision and Pattern Recognition (CVPR)*, pp. 2261–2269, 2017. doi: 10.1109/CVPR.2017.243.

Steffen Jung, Jovita Lukasik, and Margret Keuper. Neural architecture design and robustness: A dataset. In *The Eleventh International Conference on Learning Representations*, 2023.

Alex Krizhevsky. Learning multiple layers of features from tiny images. 2009. URL https://api.semanticscholar.org/CorpusID:18268744.

Alex Krizhevsky, Ilya Sutskever, and Geoffrey E Hinton. Imagenet classification with deep convolutional neural networks. In F. Pereira, C.J. Burges, L. Bottou, and K.Q. Weinberger (eds.), *Advances in Neural Information Processing Systems*, volume 25. Curran Associates, Inc., 2012. URL https://proceedings.neurips.cc/paper_files/paper/2012/file/c399862d3b9d6b76c8436e924a68c45b-Paper.pdf.

Ya Le and Xuan S. Yang. Tiny imagenet visual recognition challenge. 2015. URL https://api.semanticscholar.org/CorpusID:16664790.

Guillaume Lecué and Matthieu Lerasle. Robust machine learning by median-of-means : theory and practice, 2017. URL https://arxiv.org/abs/1711.10306.

Chao Li, Jia Ning, Han Hu, and Kun He. Adaptive channel allocation for robust differentiable architecture search. *IEEE Transactions on Neural Networks and Learning Systems*, 2024.

Yiqi Lin, Yuki Endo, Jinho Lee, and Shunsuke Kamijo. Neural architecture search via trainless pruning algorithm: A bayesian evaluation of a network with multiple indicators. *Electronics*, 13 (22), 2024. ISSN 2079-9292. doi: 10.3390/electronics13224547. URL https://www.mdpi.com/2079-9292/13/22/4547.

Aishan Liu, Shiyu Tang, Siyuan Liang, Ruihao Gong, Boxi Wu, Xianglong Liu, and Dacheng Tao. Exploring the relationship between architectural design and adversarially robust generalization. In *Proceedings of the IEEE/CVF conference on computer vision and pattern recognition*, pp. 4096–4107, 2023.

Hanxiao Liu, Karen Simonyan, and Yiming Yang. Darts: Differentiable architecture search, 2019. URL https://arxiv.org/abs/1806.09055.

Gabor Lugosi and Shahar Mendelson. Mean estimation and regression under heavy-tailed distributions–a survey, 2019. URL https://arxiv.org/abs/1906.04280.

Aleksander Madry, Aleksandar Makelov, Ludwig Schmidt, Dimitris Tsipras, and Adrian Vladu. Towards deep learning models resistant to adversarial attacks, 2019. URL https://arxiv.org/abs/1706.06083.

Joseph Mellor, Jack Turner, Amos Storkey, and Elliot J. Crowley. Neural architecture search without training, 2021. URL https://arxiv.org/abs/2006.04647.

Jisoo Mok, Byunggook Na, Hyeokjun Choe, and Sungroh Yoon. Advrush: Searching for adversarially robust neural architectures, 2021. URL https://arxiv.org/abs/2108.01289.

Utkarsh Nath, Yancheng Wang, Pavan Turaga, and Yingzhen Yang. Rnas-cl: Robust neural architecture search by cross-layer knowledge distillation. *International journal of computer vision*, 132 (12):5698–5717, 2024.

Andrzej S. Nowak and Tadeusz Radzik. The shapley value for n-person games in generalized characteristic function form. *Games and Economic Behavior*, 6(1):150–161, 1994. ISSN 0899-8256. doi: https://doi.org/10.1006/game.1994.1008. URL https://www.sciencedirect.com/science/article/pii/S0899825684710086.

Babatounde Moctard Oloulade, Jianliang Gao, Jiamin Chen, Raeed Al-Sabri, Zhenpeng Wu, and Monir Abdullah. Shapley-guided pruning for efficient graph neural architecture prediction in distributed learning environments. *Information Sciences*, 695:121695, 2025.

Yuwei Ou, Yuqi Feng, and Yanan Sun. Towards accurate and robust architectures via neural architecture search. In *2024 IEEE/CVF Conference on Computer Vision and Pattern Recognition (CVPR)*, pp. 5967–5976, 2024. doi: 10.1109/CVPR52733.2024.00570.

Nicolas Papernot, Patrick McDaniel, Ian Goodfellow, Somesh Jha, Z. Berkay Celik, and Ananthram Swami. Practical black-box attacks against machine learning, 2017. URL https://arxiv.org/abs/1602.02697.

Yameng Peng, Andy Song, Haytham M. Fayek, Vic Ciesielski, and Xiaojun Chang. Swap-nas: Sample-wise activation patterns for ultra-fast nas, 2024. URL https://arxiv.org/abs/2403.04161.

Hieu Pham, Melody Y. Guan, Barret Zoph, Quoc V. Le, and Jeff Dean. Efficient neural architecture search via parameter sharing, 2018. URL https://arxiv.org/abs/1802.03268.

Peter J. Rousseeuw and Mia Hubert. Anomaly detection by robust statistics. *WIREs Data Mining and Knowledge Discovery*, 8(2), November 2017. ISSN 1942-4795. doi: 10.1002/widm.1236. URL http://dx.doi.org/10.1002/widm.1236.

Ramprasaath R. Selvaraju, Michael Cogswell, Abhishek Das, Ramakrishna Vedantam, Devi Parikh, and Dhruv Batra. Grad-cam: Visual explanations from deep networks via gradient-based localization. *International Journal of Computer Vision*, 128(2):336–359, October 2019. ISSN 1573-1405. doi: 10.1007/s11263-019-01228-7. URL http://dx.doi.org/10.1007/s11263-019-01228-7.

Christian Simon, Piotr Koniusz, Lars Petersson, Yan Han, and Mehrtash Harandi. Towards a robust differentiable architecture search under label noise. In *Proceedings of the IEEE/CVF Winter Conference on Applications of Computer Vision*, pp. 3256–3266, 2022.

Shuoyang Sun, Kaiwen Zhang, Hao Fang, Bin Chen, Jiawei Li, Enze Huo, and Shu-Tao Xia. Robnas: Robust neural architecture search for point cloud adversarial defense. In *ICASSP 2025-2025 IEEE International Conference on Acoustics, Speech and Signal Processing (ICASSP)*, pp. 1–5. IEEE, 2025.

Yaniv Taigman, Ming Yang, Marc'Aurelio Ranzato, and Lior Wolf. Deepface: Closing the gap to human-level performance in face verification. In *2014 IEEE Conference on Computer Vision and Pattern Recognition*, pp. 1701–1708, 2014. doi: 10.1109/CVPR.2014.220.

Thanh Hai Tran, Dac Tam Nguyen, Minh Duc Ngo, Long Doan, Ngoc Hoang Luong, and Huynh Thi Thanh Binh. Kernelshap-nas: a shapley additive explanatory approach for characterizing operation influences. *Neural Computing and Applications*, pp. 1–17, 2025.

Danilo Vasconcellos Vargas, Shashank Kotyan, and SPM IIIT-NR. Evolving robust neural architectures to defend from adversarial attacks. *arXiv preprint arXiv:1906.11667*, 3, 2019.

Li W, Yao S, Wan B, Xiao L, Hou C, Zhong Y, and Zhou W. Tdnn achitecture with efficient channel attention and improved residual blocks for accurate speaker recognition. *Scientific reports*, 15 (1):23484, 2025. doi: 10.1038/s41598-025-09386-0. URL https://doi.org/10.1038/s41598-025-09386-0.

Qilong Wang, Banggu Wu, Pengfei Zhu, Peihua Li, Wangmeng Zuo, and Qinghua Hu. Eca-net: Efficient channel attention for deep convolutional neural networks. In *2020 IEEE/CVF Conference on Computer Vision and Pattern Recognition (CVPR)*, pp. 11531–11539, 2020. doi: 10.1109/CVPR42600.2020.01155.

Sanghyun Woo, Jongchan Park, Joon-Young Lee, and In So Kweon. Cbam: Convolutional block attention module, 2018. URL https://arxiv.org/abs/1807.06521.

Juntao Wu, Ziyu Song, Xiaoyu Zhang, Shujun Xie, Longxin Lin, and Ke Wang. Vision transformers beat wideresnets on small scale datasets adversarial robustness. In *Proceedings of the AAAI Conference on Artificial Intelligence*, volume 39, pp. 886–894, 2025.

Han Xiao, Ziwei Wang, Zheng Zhu, Jie Zhou, and Jiwen Lu. Shapley-nas: Discovering operation contribution for neural architecture search. In *Proceedings of the IEEE/CVF Conference on Computer Vision and Pattern Recognition (CVPR)*, 2022.

Yuhui Xu, Lingxi Xie, Xiaopeng Zhang, Xin Chen, Guo-Jun Qi, Qi Tian, and Hongkai Xiong. Pc-darts: Partial channel connections for memory-efficient architecture search. In *International Conference on Learning Representations*, 2019.

Qiancheng Yang, Yong Luo, and Bo Du. Training-free robust neural network search via pruning. In *2024 IEEE International Conference on Multimedia and Expo (ICME)*, pp. 1–6. IEEE, 2024a.

Shangshang Yang, Xiangkun Sun, Ke Xu, Yuanchao Liu, Ye Tian, and Xingyi Zhang. Hybrid architecture-based evolutionary robust neural architecture search. *IEEE Transactions on Emerging Topics in Computational Intelligence*, 8(4):2919–2934, 2024b.

Yeming Yang, Qingling Zhu, Jianping Luo, Ka-Chun Wong, Qiuzhen Lin, and Jianqiang Li. Trnas: A training-free robust neural architecture search. In *Proceedings of the IEEE/CVF International Conference on Computer Vision (ICCV)*, pp. 2336–2345, October 2025.

Zhaohui Yang, Yunhe Wang, Xinghao Chen, Boxin Shi, Chao Xu, Chunjing Xu, Qi Tian, and Chang Xu. Cars: Continuous evolution for efficient neural architecture search. In *Proceedings of the IEEE/CVF conference on computer vision and pattern recognition*, pp. 1829–1838, 2020.

Zhixiong Yue, Baijiong Lin, Xiaonan Huang, and Yu Zhang. Effective, efficient and robust neural architecture search, 2020. URL https://arxiv.org/abs/2011.09820.

Arber Zela, Thomas Elsken, Tonmoy Saikia, Yassine Marrakchi, Thomas Brox, and Frank Hutter. Understanding and robustifying differentiable architecture search. In *International Conference on Learning Representations*, 2020.

Hongyang Zhang, Yaodong Yu, Jiantao Jiao, Eric P. Xing, Laurent El Ghaoui, and Michael I. Jordan. Theoretically principled trade-off between robustness and accuracy, 2019. URL https://arxiv.org/abs/1901.08573.

Jianpeng Zhang, Xiaomin Chen, Bing Yang, Qingbiao Guan, Qi Chen, Jian Chen, Qi Wu, Yutong Xie, and Yong Xia. Advances in attention mechanisms for medical image segmentation. *Computer Science Review*, 56:100721, 2025. ISSN 1574-0137. doi: https://doi.org/10.1016/j.cosrev.2024.100721. URL https://www.sciencedirect.com/science/article/pii/S1574013724001047.

Yuming Zhang, Jun Wei Hsieh, Xin Li, Ming-Ching Chang, Chun-Chieh Lee, and Kuo-Chin Fan. MOTE-NAS: Multi-objective training-based estimate for efficient neural architecture search. In *The Thirty-eighth Annual Conference on Neural Information Processing Systems*, 2024. URL https://openreview.net/forum?id=jKLyKeZfzv.

Xun Zhou, Zhenkun Wang, Liang Feng, Songbai Liu, Ka-Chun Wong, and Kay Chen Tan. Toward evolutionary multitask convolutional neural architecture search. *IEEE Transactions on Evolutionary Computation*, 28(3):682–695, 2023.

Xun Zhou, Songbai Liu, AK Qin, and Kay Chen Tan. Evolutionary neural architecture search for transferable networks. *IEEE Transactions on Emerging Topics in Computational Intelligence*, 2024.

Barret Zoph and Quoc V. Le. Neural architecture search with reinforcement learning, 2017. URL https://arxiv.org/abs/1611.01578.

Barret Zoph, Vijay Vasudevan, Jonathon Shlens, and Quoc V. Le. Learning transferable architectures for scalable image recognition. In *2018 IEEE/CVF Conference on Computer Vision and Pattern Recognition*, pp. 8697–8710, 2018. doi: 10.1109/CVPR.2018.00907.

A Appendix

A.1 Theoretical Justification of ROSE Estimator

This appendix provides a concentration bound for the Robust Outlier-aware Shapley Estimator (ROSE) under mild assumptions.

A.1.1 ASSUMPTIONS

Assumption 1 (Bounded Marginal Gains). For any branch b, edge e, operation o, and permutation s,

$$\left|\Delta^{(s,b)}_{e,o,\mathrm{std}}\right| \le M, \qquad \left|\Delta^{(s,b)}_{e,o,\mathrm{adv}}\right| \le M, \tag{20}$$

where $M > 0$ is a finite constant. Since the Shapley value $\phi^{(b)}_{e,o}$ is a convex combination of bounded marginal gains, we also have $|\phi^{(b)}_{e,o}| \le M$.

Assumption 2 (Permutation Independence). The S Monte-Carlo permutations are sampled independently and partitioned into buckets for the MoM estimator; independence implies inter-bucket independence.

A.1.2 TRIANGLE INEQUALITY FOR ROSE SCORE

ROSE combines a Median-of-Means (MoM) estimator $m^{(b)}_{e,o}$ and an outlier-aware score $v^{(b)}_{e,o} \in [-1, 1]$:

$$\mathrm{Score}^{(b)}_{e,o} \;=\; (1-\beta)\, m^{(b)}_{e,o} \;+\; \beta\, v^{(b)}_{e,o}, \qquad 0 \le \beta < 1. \tag{21}$$

Subtracting the true Shapley value $\phi^{(b)}_{e,o}$ gives

$$\left|\mathrm{Score}^{(b)}_{e,o} - \phi^{(b)}_{e,o}\right| = \left|(1-\beta)\big(m^{(b)}_{e,o} - \phi^{(b)}_{e,o}\big) + \beta\big(v^{(b)}_{e,o} - \phi^{(b)}_{e,o}\big)\right| \tag{22}$$

$$\le (1-\beta)\left|m^{(b)}_{e,o} - \phi^{(b)}_{e,o}\right| + \beta\left|v^{(b)}_{e,o} - \phi^{(b)}_{e,o}\right|. \tag{22$'$}$$

Because $|v^{(b)}_{e,o}| \le 1$ and $|\phi^{(b)}_{e,o}| \le M$, define $C := 1 + M$ for later use.

A.1.3 PROBABILITY RELAXATION

We upper-bound the deviation probability:

$$\Pr\big(|\mathrm{Score}^{(b)}_{e,o} - \phi^{(b)}_{e,o}| \ge \varepsilon\big). \tag{23}$$

When $\varepsilon > \beta C$, inequality equation 22$'$ implies

$$|m^{(b)}_{e,o} - \phi^{(b)}_{e,o}| \;\ge\; \frac{\varepsilon - \beta C}{1-\beta}. \tag{24}$$

Hence

$$\Pr\big(|\mathrm{Score}^{(b)}_{e,o} - \phi^{(b)}_{e,o}| \ge \varepsilon\big) \;\le\; \Pr\Big(|m^{(b)}_{e,o} - \phi^{(b)}_{e,o}| \ge \tfrac{\varepsilon-\beta C}{1-\beta}\Big). \tag{25}$$

A.1.4 CONCENTRATION OF MOM ESTIMATOR

According to the MoM concentration bound (Lugosi & Mendelson, 2019), if the bucket (group) size is at least n_0, then for any $t > 0$,

$$\Pr\big(|m^{(b)}_{e,o} - \phi^{(b)}_{e,o}| \ge t\big) \;\le\; 2\exp\big(-\tfrac{n_0\, t^2}{2M^2}\big). \tag{26}$$

Plugging $t = \frac{\varepsilon-\beta C}{1-\beta}$ into equation 26 and using equation 25 yields

$$\Pr\big(|\mathrm{Score}^{(b)}_{e,o} - \phi^{(b)}_{e,o}| \ge \varepsilon\big) \;\le\; 2\exp\Big(-\frac{n_0(\varepsilon-\beta C)^2}{2M^2(1-\beta)^2}\Big). \tag{27}$$

A.1.5 FINAL RELAXATION

If $\varepsilon > 2\beta C$ then $(\varepsilon - \beta C)^2 \ge \varepsilon^2/4$ and $(1-\beta)^2 \le 1$, so

$$\Pr\big(|\mathrm{Score}^{(b)}_{e,o} - \phi^{(b)}_{e,o}| \ge \varepsilon\big) \;\le\; 2\exp\Big(-\tfrac{n_0\,\varepsilon^2}{8M^2}\Big). \tag{28}$$

$$\varepsilon > 2\beta(1+M).$$

Thus, ROSE enjoys a sub-Gaussian tail (up to a constant factor), completing the proof. Equation equation 28 establishes a sub-Gaussian tail

$$\Pr\big(|\mathrm{Score} - \phi| \ge \varepsilon\big) \le 2\exp\Big(-\tfrac{n_0\varepsilon^2}{8M^2}\Big).$$

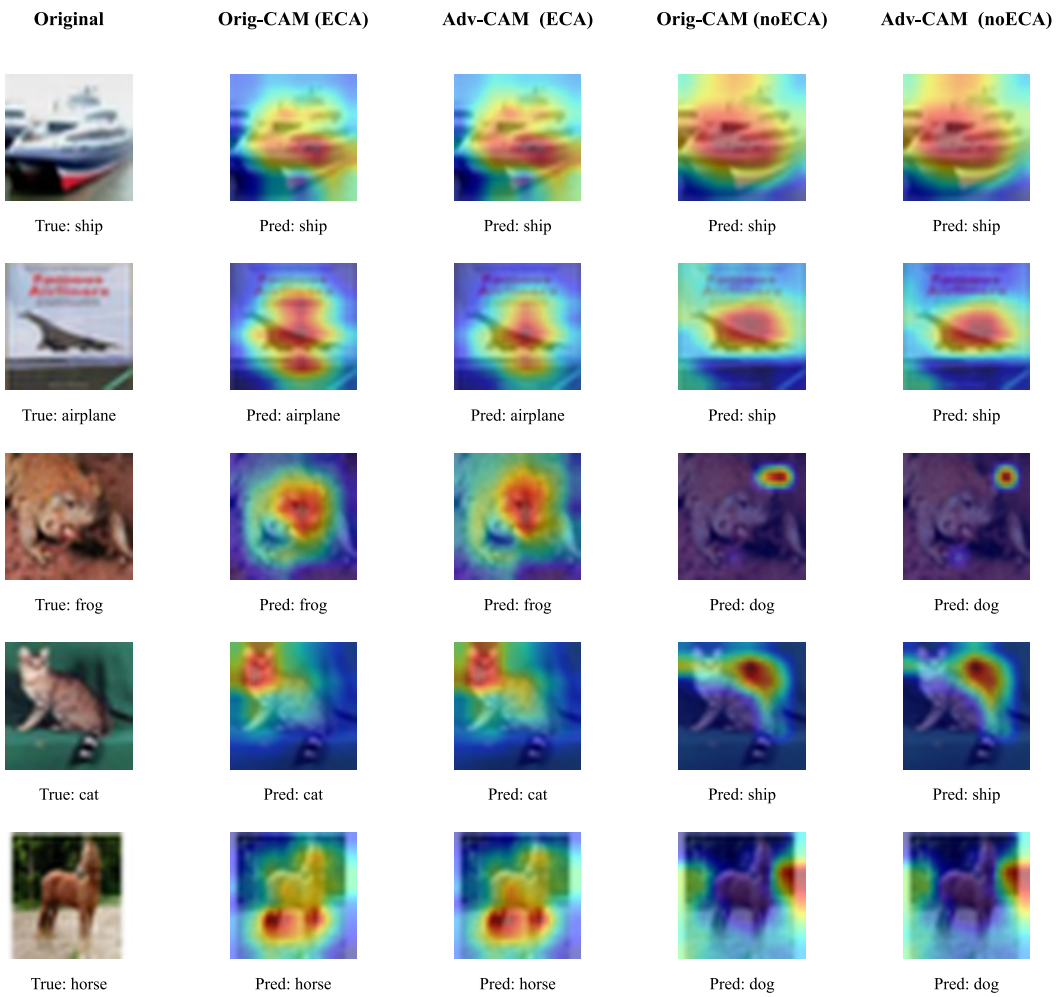

Figure 3: Grad-CAM visualizations comparing models with and without ECA under clean and adversarial inputs.

Discussion. The MoM mechanism counteracts heavy-tailed noise, while the outlier-aware term $v_{e,o}$ suppresses extreme gradients, yielding robustness even when adversarial or extreme samples are present. The guarantees rely only on inter-bucket independence and thus extend naturally to multi-GPU or multi-node distributed settings. The error–probability relation also couples the bucket size n_0 with any desired confidence level, allowing practitioners to minimize sampling—and hence search cost—while meeting accuracy targets. Finally, the coefficient β acts as a design knob between statistical reliability and outlier penalization; the theory requires $\varepsilon > 2\beta(1 + M)$, so exponentially decaying β or rescaling gains (reducing M) keeps evaluations within the admissible region, transforming heuristic "β tuning" into a quantitatively grounded procedure.Although we conduct the search with only 1k/0.5k labeled samples on CIFAR-10, our theoretical guarantees concern the *estimation* sample size used by ROSE (i.e., the number of independent evaluations per MoM bucket), rather than the dataset size itself. By increasing the number of permutations, data augmentations, and resamplings, we effectively enlarge n_0. With a small β and bounded gains (small M), the sub-Gaussian tail bound still applies—albeit with a looser constant— hence our small-data search remains consistent with the theory.

A.2 Visualization of ECA Module's Effect

To examine how the ECA (Efficient Channel Attention) module affects robustness and interpretability, we visualize class activation maps (CAMs) using Grad-CAM (Selvaraju et al., 2019) under both

clean and adversarial inputs. We use the last convolutional block for Grad-CAM, and normalize each CAM to $[0, 1]$ (per image) before overlay. Adversarial CAMs are generated with untargeted PGD-20 under ℓ_∞ budget $\epsilon = 8/255$ (step size $2/255$, random starts). Figure 3 shows a grid of five representative CIFAR-10 samples and their corresponding CAMs, using the same inputs across models for a fair comparison.

- **Column 1**: Original image with ground-truth label.
- **Columns 2–3 (with ECA)**: CAMs under clean and adversarial inputs.
- **Columns 4–5 (w/o ECA)**: CAMs for the same architecture without ECA.

We observe that models with ECA tend to produce more focused, class-consistent activation maps. For instance, in the frog example (row 3), clean and adversarial CAMs remain centered on the object when ECA is enabled, whereas the w/o-ECA counterpart exhibits a pronounced shift that coincides with a misclassification to "dog." In the cat example (row 4), the ECA model preserves attention over the cat body, while the w/o-ECA variant misclassifies it as "ship" and shifts attention to background. Similar patterns appear in the horse sample (row 5), suggesting improved stability of attention under perturbations.

Overall, these qualitative results indicate that ECA can promote both adversarial robustness and interpretability by enforcing more discriminative and stable attention over semantically meaningful regions.

A.3 Hyperparameter Settings and Search Details

To ensure fair comparison and reproducibility, we follow standard settings widely adopted in robust NAS for optimization and adversarial attacks. Unless otherwise noted, all experiments use:

- **Optimizer**: SGD with momentum 0.9, initial learning rate 0.025, cosine annealing;
- **Weight decay**: 3×10^{-4};
- **Search epochs**: 50;
- **Adversarial training**: PGD-7 with step size $2/255$ and $\epsilon = 8/255$ (untargeted, random starts; evaluation protocol in Sec. 4.2).

We only tune the two hyperparameters introduced by the **ROSE** module:

- $\boldsymbol{\beta}$: trade-off coefficient between the median-of-means (steady contribution) and the IQR-based outlier score (occasional indispensability);
- $\boldsymbol{\lambda = (\lambda_1, \lambda_2)}$: asymmetric IQR scale factors for upper/lower fences, used to detect significant outliers in clean/adv gains, respectively, with

$$\boldsymbol{\tau^+ = Q_3 + \lambda_1\,\mathrm{IQR}, \qquad \tau^- = Q_1 - \lambda_2\,\mathrm{IQR}.}$$

We conduct a lightweight grid search over:

- $\beta \in \{0,\ 0.2,\ 0.3,\ 0.4,\ 0.5,\ 1\}$;
- $(\lambda_1, \lambda_2) \in \{1.2,\ 1.5,\ 2.0\} \times \{1.2,\ 1.5,\ 2.0\}$.

Table 6 summarizes CIFAR-10 results under different (λ_1, λ_2) choices. The best-performing setting is $(\lambda_1{=}1.2,\ \lambda_2{=}2.0)$, which yields strong clean accuracy and adversarial robustness.

A.4 Cell Visualization of the Final Architecture

To enhance reproducibility and provide architectural insights, we visualize the three cell types discovered by RDNAS on CIFAR-10: the *Normal* cell, the *Reduction* cell, and the *Robust* cell. Each cell is a directed acyclic graph in which nodes denote intermediate feature maps and edges denote selected operations. Inputs c_{k-2} and c_{k-1} are the outputs of the two preceding cells, and c_k is the current cell's output. The final genotype is obtained from the discretized architecture at the end of search.

Table 6: CIFAR-10 performance under different (λ_1, λ_2) for asymmetric IQR thresholds. Best is **bold**, second best is underlined. Attacks follow Sec. 4.2.

λ_1	λ_2	Clean	FGSM	PGD^{20}	PGD^{100}
1.5	1.2	84.69%	58.41%	50.45%	50.07%
1.5	1.5	85.45%	59.55%	52.18%	51.73%
1.2	2.0	**86.56%**	**60.44%**	**52.62%**	**52.24%**
2.0	1.5	85.05%	57.74%	49.97%	49.61%

Table 7: CIFAR-10 performance under different β values. Best is **bold**. Attacks follow Sec. 4.2.

β	Clean	FGSM	PGD^{20}	PGD^{100}
0	85.25%	60.21%	52.55%	52.08%
0.2	85.06%	58.68%	50.54%	50.20%
0.3	**86.56%**	**60.44%**	**52.62%**	**52.24%**
0.4	85.49%	59.63%	52.22%	51.67%
0.5	84.83%	58.48%	50.99%	50.47%
1	84.45%	59.47%	52.45%	52.13%

- **Normal cell.** Prioritizes expressive operations (e.g., `sepconv-3x3`, `sepconv-5x5`), forming deeper computation paths while maintaining gradient flow with occasional `skipconnect`.
- **Reduction cell.** Responsible for spatial downsampling, often combining pooling (e.g., `maxpool-3x3`) with separable convolutions to expand the receptive field efficiently.
- **Robust cell.** Tends to favor smoother or more redundant topologies (e.g., `dilconv-5x5`, `skipconnect`), which are associated with improved stability under perturbations.

Together, the three cells emphasize complementary goals—expressiveness (Normal), efficiency (Reduction), and stability (Robust)—which helps explain the observed balance between clean accuracy and adversarial robustness.

A.5 Full-Scale Visualization of Primitive Trends

To provide a comprehensive view of search dynamics, we visualize the high-resolution trigger trends of each primitive in both the *Normal* and *Robust* cells across 50 search epochs. While the main paper provides compact summaries for space, the figures below reveal finer-grained patterns and fluctuations. For clarity, "exception triggers" (method-specific events such as IQR outliers) are counted per epoch; see Sec. 3.4 for the formal definition.

We observe that primitives such as `sepconv-3x3/5x5` and `dilconv-5x5` are *often* among the most frequently triggered in both cells, suggesting their importance for robust architecture formation. In contrast, `skipconnect` and pooling operations (e.g., `avgpool-3x3`, `maxpool-3x3`) are triggered less frequently, indicating a lower tendency to be prioritized in our robustness-aware search space.

The temporal curves also exhibit periodic rises and falls, implying that the search revisits and reassesses operator importance over time rather than converging prematurely. These detailed trends support the effectiveness of our ROSE-based exception mechanism in tracking meaningful shifts in primitive utility.

A.6 Attention Module Selection

To assess how the fusion attention choice shapes both the searched architecture and robustness, we evaluate three candidates—CBAM (reduction$=16$, k=7) (Woo et al., 2018), ECAM (k_c=3, k_s=5) (W et al., 2025), and ECA (k=3) (Wang et al., 2020; Zhang et al., 2025)—by replacing the attention module in the search space and re-running the full NAS pipeline for each variant. Apart

Table 8: Attention module comparison on CIFAR-10 (%, ℓ_∞, $\epsilon = 8/255$, PGD step size $2/255$). Single run per setting; best in each column is **bold**.

Module	Params (M)	Clean	FGSM	$\mathbf{PGD^{20}}$	$\mathbf{PGD^{100}}$	$\mathbf{APGD_{CE}}$
CBAM (reduction=16, k=7)	4.2	84.62	59.72	52.38	51.99	51.73
ECAM ($k_c = 3$, $k_s = 5$)	4.5	<u>85.34</u>	<u>59.92</u>	<u>52.57</u>	<u>52.17</u>	<u>51.95</u>
ECA ($k = 3$)	4.4	**86.56**	**60.44**	**52.62**	**52.24**	**52.05**

from the attention module, all factors are held fixed: the rest of the primitives, random seeds and splits, search/training budgets, and optimization hyperparameters (including 7-step PGD adversarial training with step size $2/255$, ϵ=$8/255$).

As reported in Table 8, under the "re-search + retrain" setting, ECA yields the best or tied-best performance across all metrics. ECAM (a spatially-extended ECA) is close under strong attacks but slightly behind overall; CBAM drops further under stronger attacks. Because the resulting models have nearly identical parameter counts, these gains are unlikely to stem from model size, pointing instead to how attention design shapes the searched topology and robustness-oriented inductive bias.

Why does ECA lead the search? We believe three factors contribute: (1) No channel bottleneck: ECA's local 1D channel convolution avoids MLP reduction, preserving fine-grained discriminative information that is easily lost under adversarial training; (2) Local channel neighborhoods: small-kernel cross-channel interactions appear more stable to perturbation noise, reducing variance in Shapley-style scoring and gradient updates during search; (3) Lightweight and optimization-friendly: with minimal parameters and a short optimization path, ECA couples more benignly with adversarial losses, whereas spatial branches and strong reduction (CBAM/ECAM) add compute and can aggravate optimization instability without consistent robustness gains.

A.7 Robustness Across PGD Budgets

To examine how robustness evolves with the strength of the adversary, we sweep the perturbation budget ϵ for untargeted L_∞ PGD on CIFAR-10 and evaluate all models under a fixed, transparent protocol:

- **Attack setup.** For each $\epsilon \in \{1, 2, 3, 4, 6, 8\}/255$ we use step size $\alpha = \epsilon/4$, $r = 5$ random restarts with uniform initialization in the ℓ_∞ ball, and T PGD iterations. To avoid under-optimized attacks at small budgets, T is increased as ϵ decreases (Table 9). No attack parameter is tuned per model.

- **Evaluation.** Robust accuracy is measured on the full test set; images are clipped to $[0, 1]$ after each step. The same settings are applied to all compared methods.

Results and takeaways. Table 9 reports the robust accuracy grid. As expected, accuracy decreases monotonically as ϵ grows. Across the full range of budgets, **RDNAS** consistently matches or exceeds baselines, with the largest margins appearing at the higher budgets (e.g., $\epsilon = 8/255$). At moderate budgets ($\epsilon \in [3, 6]/255$), RDNAS preserves a comfortable robustness headroom while maintaining competitive clean accuracy (see main text), indicating that its dual-branch design and ECA fusion do not rely on a narrow operating point.

All runs use identical preprocessing, evaluation code, and random seeds across models. We follow the common choice $\alpha = \epsilon/4$ and keep restarts fixed ($r = 5$) to balance attack strength and runtime. This grid can serve as a drop-in stress test for future methods to report budget sensitivity under a standardized PGD protocol.

Table 9: Robust accuracy (%) under L_∞ PGD with varying budgets. Default $\alpha = \epsilon/4$, restarts $r = 5$.

ϵ	α	T	r	**RDNAS(Ours)**	**LRNAS**	**RACL**	**AdvRush**
$8/255$	$2/255$	20	5	**52.62**	50.20	51.89	52.29
$6/255$	$1.5/255$	20	5	**62.84**	56.05	61.94	62.09
$4/255$	$1/255$	20	5	**72.11**	66.45	71.33	71.94
$3/255$	$0.75/255$	30	5	**76.08**	71.05	75.33	75.49
$2/255$	$0.5/255$	40	5	**79.91**	75.12	79.87	79.70
$1/255$	$0.25/255$	50	5	**83.34**	79.29	82.24	83.14

A.8 Robustness across various sample typeson CIFAR-10 under ℓ_∞ Attacks

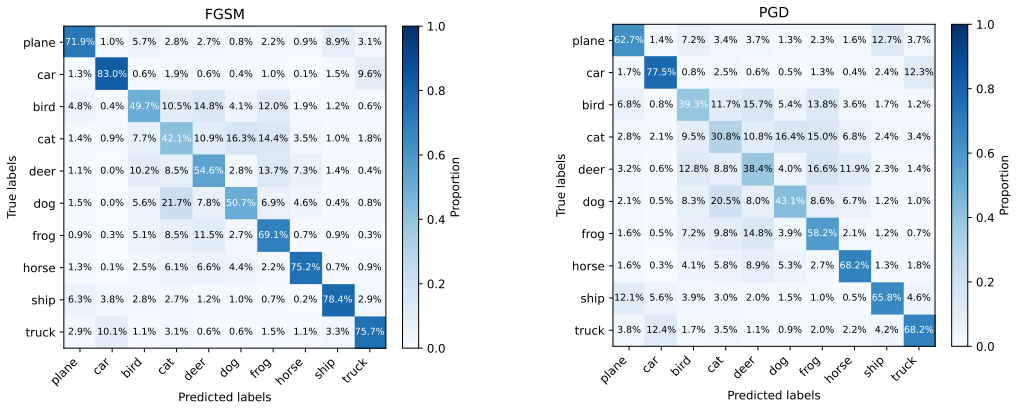

(a) FGSM, $\epsilon = 8/255$.

(b) PGD^{20}, $\epsilon = 8/255$.

Figure 7: Class-wise confusion matrices of the final RDNAS model on CIFAR-10 under white-box ℓ_∞ attacks.

To better understand why a robust estimator like ROSE is needed in our adversarial NAS setting, we report class-wise confusion matrices of the final RDNAS model on **CIFAR-10** under **white-box ℓ_∞ attacks** in Figure 7.

Dataset: CIFAR-10 test set (10,000 images, 10 classes).
Model: The final RDNAS architecture adversarially trained
Attacks:

- **FGSM** (ℓ_∞) with perturbation budget $\epsilon = 8/255$.
- **PGD**^{20} (ℓ_∞) with $\epsilon = 8/255$, step size $2/255$, 20 steps, and random starts.

Figure 7 reveals a clear heterogeneity across classes: some classes (e.g., *bird, cat, deer, dog*) suffer substantial drops in diagonal accuracy and much larger mass spread over incorrect labels, whereas others (e.g., *plane, car, frog, horse, ship, truck*) remain comparatively robust under the same attack budget. This behavior indicates that, even at a fixed ℓ_∞ budget on CIFAR-10, the induced adversarial loss distribution is **highly skewed and class-dependent**. A relatively small subset of "hard" examples and vulnerable classes contributes disproportionately to the gradients, leading to **heavy-tailed and occasionally extreme** marginal gains when estimating operation-level Shapley values in a weight-sharing supernet. In such a regime, naive averaging of marginal gains can be dominated by these outliers and yield unstable operation rankings across runs. ROSE explicitly addresses this issue by combining (i) a **Median-of-Means** term, which provides a robust estimate of the typical contribution under heavy-tailed noise, and (ii) an **IQR**-based component, which controls the influence of rare but extreme deviations. The CIFAR-10 confusion matrices in Figure 7 thus provide empirical motivation for using ROSE as a robust operation-scoring mechanism in adversarial NAS.

A.9 Additional ImageNet-1k Experiments

Following TRNAS (Yang et al., 2025), we train all architectures on ImageNet-1k with FAST-FGSM adversarial training for 50 epochs, perturbation radius $\epsilon = 4/255$, and SGD with momentum. We use a batch size of 512 and apply the same training protocol to DARTS (Liu et al., 2019), LR-NAS (Feng et al., 2025a), CRoZe (Ha et al., 2023), ZCPRob (Feng et al., 2025b), TRNAS, and our searched architecture. After training, we report top-1 accuracy on clean images, FGSM, and PGD-20 attacks.

Table 10: Comparison of NAS methods on ImageNet-1k under FAST-FGSM training ($\epsilon = 4/255$). We report top-1 accuracy (%).

Methods	Type	Clean	FGSM	PGD-20
DARTS	Clean	53.88	19.22	11.11
LRNAS	Robust	48.21	15.02	8.18
CRoZe	Zero-shot robust	49.52	16.28	9.41
ZCPRob	Zero-shot robust	52.93	18.86	10.75
TRNAS	Zero-shot robust	55.10	20.56	11.73
Ours	Robust	**57.09**	**22.11**	**12.68**

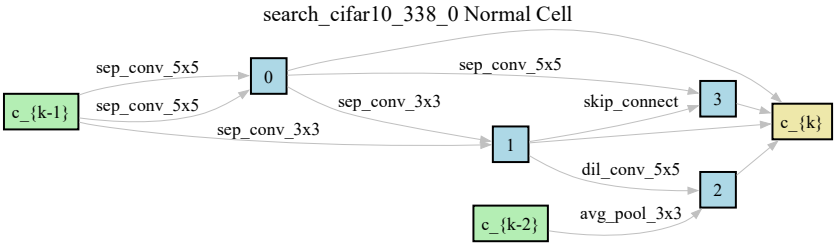

(a) Normal cell discovered by RDNAS on CIFAR-10.

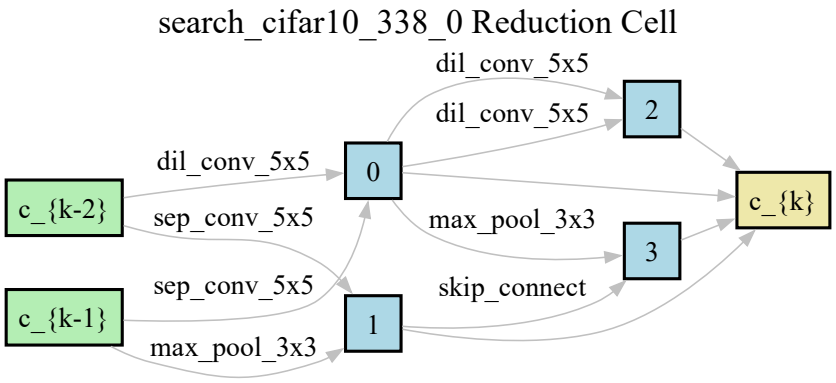

(b) Reduction cell discovered by RDNAS on CIFAR-10.

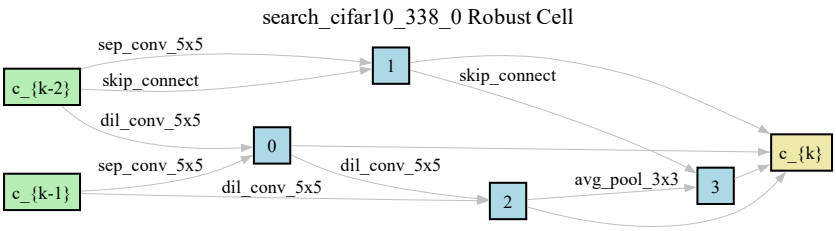

(c) Robust cell discovered by RDNAS on CIFAR-10.

Figure 4: Cells discovered by RDNAS on CIFAR-10. From top to bottom: Normal, Reduction, and Robust cells.

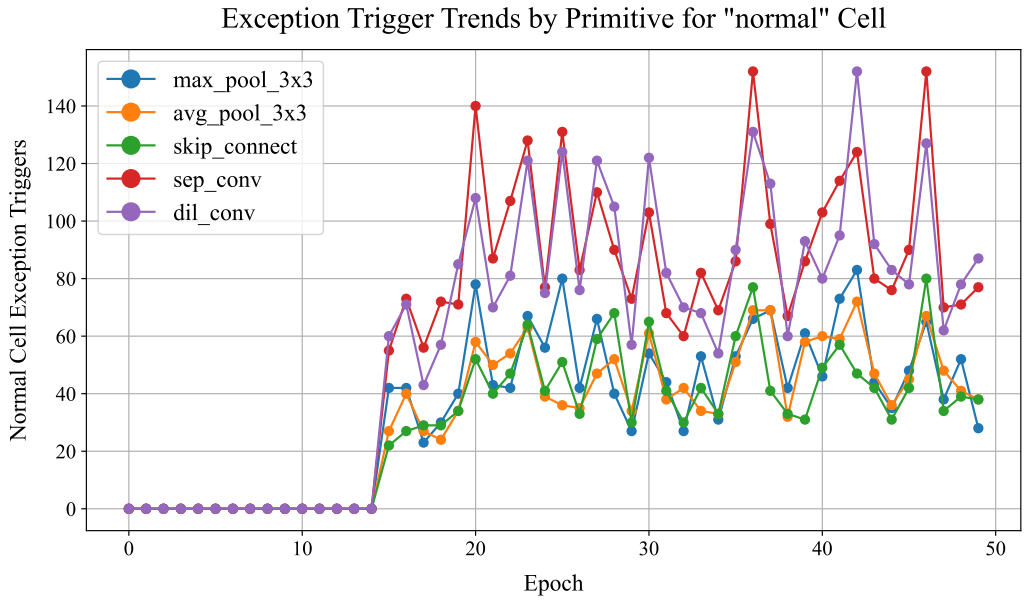

Figure 5: High-resolution trigger trends for primitives in the Normal cell across 50 search epochs.

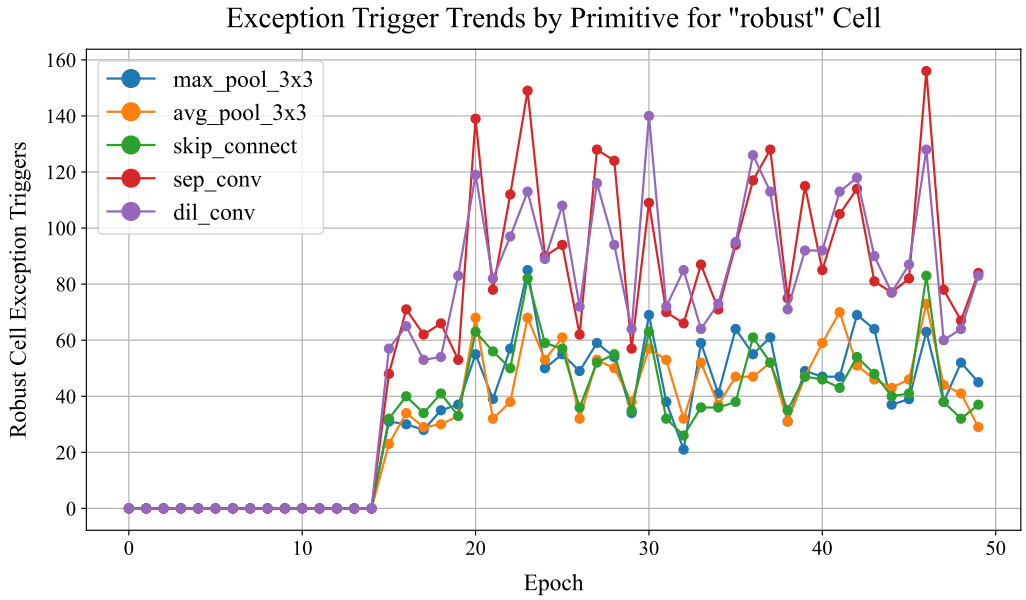

Figure 6: High-resolution trigger trends for primitives in the Robust cell across 50 search epochs.